

Raining Rocks: An analytical formulation for collision timescales in planetary systems

Santiago Torres,^{1,2*} Smadar Naoz,^{1,2} Gongjie Li³ and Sanaea C. Rose^{1,2}

¹*Department of Physics and Astronomy, University of California, Los Angeles, CA 90095, USA*

²*Mani L. Bhaumik Institute for Theoretical Physics, University of California, Los Angeles, CA 90095, USA*

³*Center for Relativistic Astrophysics, School of Physics, Georgia Institute of Technology, Atlanta, GA 30332, USA*

Accepted XXX. Received YYY; in original form ZZZ

ABSTRACT

The dynamical interaction of minor bodies (such as comets or asteroids) with planets plays an essential role in the planetary system’s architecture and evolution. As a result of these interactions, structures like the Kuiper belt and the Oort cloud can be created. In particular, the collision of minor bodies with planets can drastically change the planet’s internal and orbital evolution. We present an analytic formulation to determine the collision timescale for a minor body to impact a planet for arbitrary geometry. By comparing with a suite of detailed N-body simulations and an analytical method for collision timescales in the solar system, we confirmed the accuracy of our analytic formulation. As a proof of concept, we focused on the collision rate of minor bodies randomly distributed around a Jupiter-like planet, emulating a Kuiper belt-like disk. We show that our analytical method yields in good agreement with the numerical simulations. The formalism presented here thus provides a succinct and accurate alternative to numerical calculations.

Key words: orbital dynamics, comets and asteroids, cometary impacts

1 INTRODUCTION

Minor bodies such as comets and asteroids in the solar system are remnants of the planet formation process (Kokubo & Ida 2002; Kenyon & Bromley 2006; Wyatt 2008; Johansen & Lambrechts 2017). These objects play an important role in the evolution of their planetary system (Nesvorný 2018; Torres et al. 2019; Cai et al. 2019). In particular, the dynamical evolution of these bodies in any planetary system is dominated by the gravitational interaction with major bodies such as the planets. As the comets come close to planetary regions, planets become the main influence for these objects.

Thus, gravitational interactions with planets, such as close encounters and collisions, may have influenced the planets’ history, composition, structure, and evolution (Asphaug et al. 2006; Brasser et al. 2020; Morgan et al. 2021). Examples of these processes include cometary impacts that may be responsible for the dawn-dusk asymmetry of Mercury’s exosphere (e.g., Benz et al. 1988; Pokorný et al. 2017), the changes of the surface and atmosphere on Mars (e.g., Carr 1989; Melosh & Vickery 1989; Woo et al. 2019), and the dynamical evolution of the gas giants and trans-neptunian objects ((Gomes et al. 2005; Muñoz-Gutiérrez et al. 2021), for more examples see Stern (1995); Marov & Rickman (2001); Charnoz & Morbidelli (2003). Furthermore, collisions with these remnants may have a dramatic effect on a planet’s orbit. For example, repeated collisions may have resulted in the tilt of Uranus (e.g., Brunini 1995; Parisi & Brunini 1997; Rogoszinski & Hamilton 2021). Lastly, the Chicxulub impact on Earth is suspected to be the main cause of the

extinction of the dinosaurs (e.g., Alvarez et al. 1980; Schulte et al. 2010).

Cometary (and other minor body) impacts in the solar system have been extensively studied in the literature (e.g., Opik 1951; Kessler 1981; Greenberg et al. 1988; Bottke & Greenberg 1993; Marov & Rickman 2001; Muinonen et al. 2001; Valsecchi 2005; Rickman et al. 2014). Of particular interest is the impact rate of comet collisions with planets. These calculations are often based on the Öpik’s analytic method (Opik 1951). However, these methods are often tuned to model cometary impacts in the inner part of the solar system. As a result, it is challenging to calculate collision rates in other planetary systems with different architectures, arbitrary configurations and geometries than the solar system.

Here we present a succinct and accurate model to calculate the collisions rate and timescale for a minor body to impact a planet. Our methodology is applicable for all geometries and configurations and is consistent with direct numerical calculations. In Sect. 2, we present our model for collisional timescales. In Sect. 3 we test our model by comparing our predictions with a well known analytic method for collision rates in the solar system and detailed N-body simulations. Finally, we discuss our results in Sect. 4.

2 COLLISIONAL TIMESCALES FOR PARTICLE IMPACTS ON PLANETS

Here we present a general analytical approach, to calculate the collision rate of a minor body with a planet for arbitrary geometry of interaction. Hereafter we refer to a minor body as a particle to highlight the wide range of application.

* E-mail: storres@astro.ucla.edu

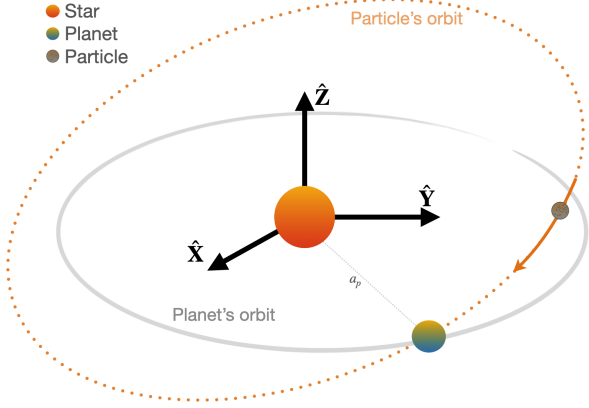


Figure 1. Orbital motion of a particle about its host star with respect to the planet's orbital plane. The semi-major axis of the planet is given by a_p .

Consider the collision rate, Γ_{coll} (Eq. (1)), of a particle with a planet. This rate can be calculated by assuming a population of planet-orbital-crossing particles a with number density n that will eventually collide with the planet. The relative velocity between the planet and the particle (v_{rel}), and the cross section of interaction (σ). We assume an arbitrary configuration for the planet and particle; see Fig. 1 for illustration. Thus, the collision rate can be approximated as (e.g., Binney & Tremaine 2008; Nesvorný et al. 2020; Rose et al. 2020)

$$\Gamma_{\text{coll}} = n v_{\text{rel}} \sigma. \quad (1)$$

The number density is then simply $n = N_c/V$, where N_c is the number of colliding particles and V is the volume where collision can take place, and is given by,

$$V = 2\pi^2 a_p R_p^2 \sin i_c, \quad (2)$$

where a_p and R_p are the semi-major axis and radius of the planet respectively and i_c is the inclination of the particle.

The relative velocity magnitude between the particle and the planet is given by the magnitude difference between the velocity vector of the planet \mathbf{v}_p and the particle \mathbf{v}_c , in other words, $v_{\text{rel}} = |\mathbf{v}_{\text{rel}}| = |\mathbf{v}_p - \mathbf{v}_c|$. To obtain the velocity vectors of the planet and the particle, we first need to establish the geometry of the encounter. We considered a reference plane in which the planet is at the center. The orbital motion of the particle about the star with respect to the center is in three-dimensional space.

The position vector of the particle in the frame of its bound orbit about the host star is: $\mathbf{r}_c = x \hat{\mathbf{x}} + y \hat{\mathbf{y}} + z \hat{\mathbf{z}}$, where $x = r_c \cos f_c$, $y = r_c \sin f_c$, $z = 0$. Where f_c is the true anomaly of the particle, and r_c is given by:

$$r_c = a_c \frac{1 - e_c^2}{1 + e_c \cos f_c}. \quad (3)$$

Then, the position vector projected to the plane of the planet is given by $\mathbf{R}_1 \mathbf{R}_2 \mathbf{R}_3 \mathbf{r}_c$, where \mathbf{R}_j , $j = 1, 2, 3$ are the rotation matrices given by (e.g., Murray & Dermott 2000),

$$\begin{aligned} \mathbf{R}_1 &= \begin{pmatrix} \cos \omega & -\sin \omega & 0 \\ \sin \omega & \cos \omega & 0 \\ 0 & 0 & 1 \end{pmatrix}, \mathbf{R}_2 = \begin{pmatrix} 1 & 0 & 0 \\ 0 & \cos i & -\sin i \\ 0 & \sin i & \cos i \end{pmatrix}, \\ \mathbf{R}_3 &= \begin{pmatrix} \cos \Omega & -\sin \Omega & 0 \\ \sin \Omega & \cos \Omega & 0 \\ 0 & 0 & 1 \end{pmatrix}. \end{aligned} \quad (4)$$

Therefore, the components of the position vector of the particle projected on the planet's can be calculated by,

$$\begin{pmatrix} X \\ Y \\ Z \end{pmatrix} = \mathbf{R}_1 \mathbf{R}_2 \mathbf{R}_3 \begin{pmatrix} x \\ y \\ z \end{pmatrix} \quad (5)$$

Consequently, the velocity vectors of the particle (\mathbf{v}_c) and the planet (\mathbf{v}_p) in their own individual orbital planes at any give time are given by

$$\mathbf{v}_{c,p} = \left(-\frac{h_{c,p} \sin f_{c,p}}{a_{c,p} (1 - e_{c,p}^2)}, \frac{h_{c,p} (e_{c,p} + \cos f_{c,p})}{a_{c,p} (1 - e_{c,p}^2)}, 0 \right), \quad (6)$$

where, the subscript c and p stands for the particle and the planet respectively. The specific angular momentum of the particle (planet) h_c (h_p) is given by,

$$h_{c,p} = \sqrt{G (M_s + M_p) a_{c,p} (1 - e_{c,p}^2)}, \quad (7)$$

where a_c (a_p), e_c (e_p) and f_c (f_p), are the semi-major axis, eccentricity and true anomaly of the particle (planet). Additionally, M_s and M_p are the mass of the star and the planet respectively. Thus, the relative velocity is given by:

$$v_{\text{rel}} = |\mathbf{v}_p - \mathbf{R}_1 \mathbf{R}_2 \mathbf{R}_3 \mathbf{v}_c|. \quad (8)$$

Where recall that we are rotating the particle velocity vector to the planet frame using $\mathbf{R}_1 \mathbf{R}_2 \mathbf{R}_3$. The relative velocity between the particle and the planet is calculated at the moment of collision. The collision of the particle with the planet takes place at the node, where the cometary orbital plane and the planet's plane coincide.

Finally, the cross section σ , enhanced by gravitational focusing, is given by:

$$\sigma = \pi \left(R_p^2 + R_p \frac{2 G M_p}{v_{\text{rel}}^2} \right), \quad (9)$$

Substituting equations 2, 8, and 9 into Eq. (1) we obtain a final expression for the collision rate per year as a function of the particle's orbital elements $\Gamma_{\text{coll}}(a_c, e_c, i_c, \Omega_c, \omega_c, f_c)$:

$$\Gamma_{\text{coll}} = \frac{N_c}{2\pi^2 a_p R_p^2 \sin i_c} \left(v_{\text{rel}} \pi R_p^2 + \pi R_p \frac{2 G M_p}{v_{\text{rel}}} \right) \quad (10)$$

Equation 10 represents the most general expression for a collision between a minor body and a planet in an arbitrary geometry.

3 COMPARISON WITH ANALYTIC AND NUMERICAL METHODS

In this section we tested our model by comparing it with the often use Öpik method for collisions in the solar system (see also Appendix B) and with detailed N-body simulations (Sec.3.3).

[h!]

3.1 The Öpik Method

The Öpik method (Öpik 1951) in its original form provides an expression for the collision rate of particles (asteroids or comets) with planets. In this 1951 method, the planet is assumed to be fixed in space in a circular orbit and the colliding particle on an arbitrary orbit. The collision happened when the orbit of the two bodies intersect. The Öpik method assumes a restricted 3-body problem, considering the small body massless and moving on an unperturbed heliocentric Keplerian orbit.

The Öpik method considers two main parts to calculate the collision rate: the relative velocity between the particle and the planet and the collisional area or cross-section. The Öpik method often uses units $G = 1$ and assumes the star's mass $M_s = 1 M_\odot$.

The reference frame is set so that the particle is at one of the nodes of its orbit when the encounter with the planet occurs. Therefore, the relative velocity U_{opik} can be expressed in terms of the Tisserand parameter with respect to the planet and is given by (e.g., Öpik 1951; Carusi et al. 1990),

$$U_{\text{opik}} = \sqrt{3 - T}, \quad (11)$$

where T , is the Tisserand parameter which is defined as,

$$T = \frac{a_p}{a_c} + 2 \cos i_c \sqrt{\frac{a_c}{a_p} (1 - e_c^2)}. \quad (12)$$

The relative velocity components, U_x , U_y , and U_z are given by (see e.g., Carusi et al. 1990),

$$\begin{aligned} U_x &= \pm \sqrt{2 - 1/a_c - a_c(1 - e_c^2)}, \\ U_y &= \sqrt{a_c(1 - e_c^2)} \cos i_c - 1, \\ U_z &= \pm \sqrt{a_c(1 - e_c^2)} \sin i_c. \end{aligned} \quad (13)$$

When a particle reaches the Hill's sphere of a planet, the Sun's perturbations can be neglected, and the trajectory of the particle can be modeled as a planetocentric. Once inside of the Hill's region, a particle can collide with the planet if the pericenter distance of the particle q_c is smaller or similar to the radius of the planet R_p , i.e., $q_c \leq R_p$. Therefore the cross-section for interaction can be expressed by σ_{opik} (e.g., Öpik 1951, 1976),

$$\sigma_{\text{opik}} = R_p \sqrt{1 + \frac{2GM_p}{U_{\text{opik}}^2 R_p}}. \quad (14)$$

With the expression for the encounter velocity U_{opik} and the cross-section σ_{opik} , the collision rate per year as a function of the particle's orbital elements $\Gamma_{\text{opik}}(a_c, e_c, i_c)$ is calculated as followed.

The Öpik method considers a particle in a heliocentric orbit, which crosses two times a sphere of radius $r = 1$. The radial velocity of the particle is U_x . Then the time spent of the particle in the sphere is $dt = 2dr/U_x$. The number of particles N_c in the sphere per orbital revolution can be calculated as $N_c = dt/P$, where P is the particle's orbital period. Öpik (1951) showed that a particle could only be found inside a band with two parallel latitudes $\pm i$ and a volume $dV = 4\pi \sin i dr$. Thus, the collision rate of a particle can be expressed by (see e.g., Öpik 1976, for a detailed derivation),

$$\Gamma_{\text{opik}} = \frac{\sigma_{\text{opik}}^2 U_{\text{opik}}}{\pi \sin i_c |U_x|}. \quad (15)$$

Despite the simplicity, the Öpik's method yields consistent results for Jupiter-family comets (e.g., Greenberg et al. 1988; Nakamura & Kurahashi 1998; Dones et al. 1999). However, it fails to accurately

Table 1. Input orbital elements of the particle and planet in the numerical simulations: a_c , e_c , i_c , Ω_c , ω_c , and f_c , f_p represents the semi-major axis, eccentricity, inclination, longitude of the ascending node, argument of periaapsis, and true anomaly of the particle and the planet, respectively.

name	e_c	a_c [au]	i [deg]	Ω_c [deg]	ω_c [deg]	f_c [deg]	f_p [deg]
R-inc	0.5	5.5	0 – 180	0	0	0	0
R-ecc	0 – 1	5.5	27.5	0	0	0	0

model the collision rate for those particles with Tisserand parameter $T \geq 3$.

Many improvements in Öpik original theory have been done by several authors (e.g., Nakamura & Kurahashi 1998; Manley et al. 1998; Dones et al. 1999; Levison et al. 2000; Zahnle 2001; Vokrouhlický et al. 2012; Pokorný & Vokrouhlický 2013; Rickman et al. 2014; JeongAhn & Malhotra 2017; Vokrouhlický et al. 2019; Abedin et al. 2021), creating a variety of Öpik-like models that address some of the existing issues of the classic method. These Öpik like-methods represent a quick (but at times less accurate) alternative to more robust numerical simulations. However, these expansions are mainly tuned for objects in the inner parts of the solar systems and they lack the flexibility to model minor bodies in exo-planetary systems for a wide range of configurations.

3.2 Numerical Method

We used the N-body package REBOUND (Rein & Liu 2012) with the WH-Fast integrator (Rein & Liu 2012) to calculate the collisional history of minor bodies with a planet. We considered a system composed by a solar mass star and a Jupiter-like planet with semi-major axis $a_p = 5.2$ au, eccentricity $e_p = 0.05$, mass $M_p = 0.001 M_\odot$. We used an inflated collisional radius $R_p = (M_p/3M_\star)^{1/3} a_p$ (to assure more collisions in shorter time). We added 5000 test particles representing the minor bodies. To compare the numerical simulation with the analytical calculation we construct two representative runs (see Appendix C). In one, **R-inc**, we vary only the initial inclination but keep all of the other orbital parameters constant, and in the other, **R-ecc** we vary only the initial eccentricity of the particle. The full set of initial conditions are described in Table 1. We model the collision of the particles as inelastic encounters. For simplicity, every particle that collided with the planet was removed from the simulation. The simulation was run up to 10^4 yrs. We note that the number of collisions does not converge on this timescale. As a function of time, the number of particles that undergo collisions increases, as expected. We performed a series of tests using a simulation time of 10^5 yrs, and we did not find qualitatively change our results. In Appendix C we show the results of the simulations.

3.3 Comparison with Analytic and Numerical Methods

In Fig. 2, we show the average collision rate from the simulation, for different eccentricity and inclination bins (orange solid line). We compare the numerical result with the calculated Γ_{coll} and Γ_{opik} (red dash-dot and blue dotted lines, respectively). We note that in both cases we use the orbital parameters of the particles at the onset of collision. Before the particles collided their orbit evolves as expected from three-body evolution (e.g., Naoz et al. 2017), thus, their initial conditions from Table 1 differs from their orbital parameters when they collide.

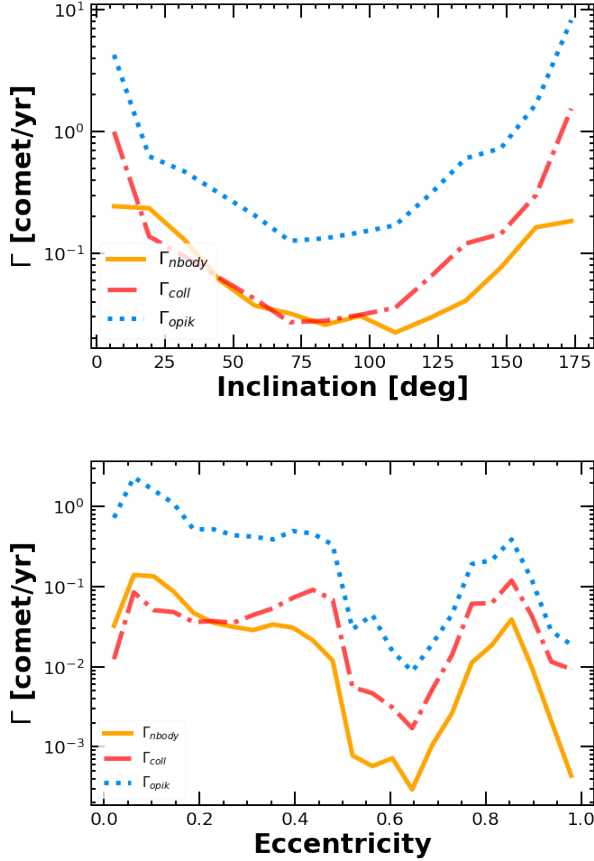


Figure 2. Comparison between the N-body simulation (solid orange line), the Öpik method (dotted blue line) and the Γ_{coll} (dash-dot red line). The top panel shows the collision rate as a function of the inclination using the values for **R-inc** listed in Table 1. While the bottom panel shows the distribution for **R-ecc** and the collision rate as a function of the eccentricity.

As depicted in Fig. 2, our analytical rate calculation, Γ_{coll} is consistent with the N-body rate in both its functional form and value.

Note that Γ_{opik} is at times few orders of magnitude different than the numerical results. Furthermore, as clearly seen in Fig. 2, Γ_{opik} estimated higher collision rate for circular orbits, at odds with the numerical and Γ_{coll} estimations.

4 SUMMARY AND DISCUSSION

Here we present an analytical model to determine the collision rate of a minor body (particle) with a planet for any type encounter geometry and orbit (Eq. (10)). We tested our formulation by comparing with the Öpik method (Sect. 3.1) and detailed N-body simulations (Sect. 3.2). As a proof of concept we choose two representative examples, one for which we vary the colliding particles eccentricities, and the other, by varying their inclinations. Our prediction for the collision rate of a particle impacting a planet is consistent with the simulations, but differ with the Öpik method.

The inconsistency between our model and the Öpik method are mainly due to the singularities produced by the Öpik method not present in our model. The Öpik method fails to estimate the collision rate for those particles with small values of inclination and $|U_x|$,

producing a singularity since Eq. (A4) goes to infinity (see Fig. B1). Therefore bodies similar to the centaurs, nearly isotropic and long-period comets, can not be accurately model following Eq. (A4). These objects are expected to be abundant in exo-planetary systems as a consequence of planet formation (e.g., Wyatt 2008; Johansen & Lambrechts 2017). On the other hand, Γ_{coll} produces better estimations for the collision rate for all varieties of orbital elements. This is because we allow for arbitrary geometry. As a result, the function Γ_{coll} allows us to model any type of minor body orbits given the flexibility to estimate collisional rates in exo-planetary systems accurately.

We note that the Öpik-like methods might provide better estimations than the original one (e.g., Valsecchi 2005; JeongAhn & Malhotra 2017; Vokrouhlický et al. 2019; Abedin et al. 2021). However, a detailed comparison with the variations of the method is beyond the scope of our paper. We omit these comparisons because our intention is not to adapt or extend the Öpik theory for collisions to any exo-planetary system. Therefore, we focus on a simple comparison with the backbone of the theory, the classic Öpik method (Öpik 1976).

Our formulation Γ_{coll} provides a succinct solution to determine the collision rate of a particle as a function of its orbital elements ($\Gamma_{\text{coll}}(a_c, e_c, i_c, \Omega_c, \omega_c, f_c)$). These allowed us to model the collision of particles with planets for any encounter geometry and orbit, providing an accurate alternative to costly N-body simulations.

ACKNOWLEDGMENTS

ST expresses his gratitude to Ylva Göteborg and Erez Michaely, for their helpful discussions and comments to the present work. ST, SN, GL thank NASA-ATP: AWD-000836-G1. Furthermore, ST and SN thank partial support from the NSF through grant No. AST-1739160 and Howard and Astrid Preston for their generous support. SR thank NASA-ATP grant number 80NSSC20K0505, as well as Nina Byers Fellowship and Michael A. Jura Memorial Graduate Award for support.

DATA AVAILABILITY

The python scripts used to generate the data for this work can be accessed here: <https://santiago-torres.com/Research>

REFERENCES

- Abedin A. Y., et al., 2021, *The Astronomical Journal*, 161, 195
 Alvarez L. W., Alvarez W., Asaro F., Michel H. V., 1980, *Science*, 208
 Asphaug E., Agnor C. B., Williams Q., 2006, *Nature*, 439, 155
 Benz W., Slattery W. L., Cameron A., 1988, *Icarus*, 74, 516
 Binney J., Tremaine S., 2008, *Galactic Dynamics*. Princeton University Press, doi:10.2307/j.ctvc778ff, <http://www.jstor.org/stable/10.2307/j.ctvc778ff>
 Bottke W. F., Greenberg R., 1993, *Geophysical Research Letters*, 20, 879
 Brassier R., Werner S., Mojszsis S., 2020, *Icarus*, 338, 113514
 Brunini A., 1995, *Planetary and Space Science*, 43, 1019
 Cai M. X., Portegies Zwart S., Kouwenhoven M. B. N., Spurzem R., 2019, *Monthly Notices of the Royal Astronomical Society*, 489, 4311
 Carr M. H., 1989, *Icarus*, 79, 311
 Carusi A., Valsecchi G. B., Greenberg R., 1990, *Celestial Mechanics and Dynamical Astronomy*, 49, 111
 Charnoz S., Morbidelli A., 2003, *Icarus*, 166, 141
 Dones L., Gladman B., Melosh H. J., Tonks W. B., Levison H. F., Duncan M., 1999, *Icarus*, 142, 509

Gomes R., Levison H. F., Tsiganis K., Morbidelli A., 2005, *Nature*, 435, 466
 Greenberg R., Carusi A., Valsecchi G., 1988, *Icarus*, 75, 1
 JeongAhn Y., Malhotra R., 2017, *The Astronomical Journal*, 153, 235
 Johansen A., Lambrechts M., 2017, *Annual Review of Earth and Planetary Sciences*, 45, 359
 Kenyon S. J., Bromley B. C., 2006, *The Astronomical Journal*, 131, 1837
 Kessler D. J., 1981, *Icarus*, 48, 39
 Kokubo E., Ida S., 2002, *The Astronomical Journal*, 581, 666
 Levison H. F., Duncan M. J., Zahnle K., Holman M., Dones L., 2000, *Icarus*, 143, 415
 Manley S. P., Migliorini F., Bailey M. E., 1998, *Astronomy and Astrophysics Supplement Series*, 133, 437
 Marov M. Y., Rickman H., 2001, *Paper Knowledge . Toward a Media History of Documents*, 261
 Melosh H. J., Vickery A. M., 1989, *Nature*, 338, 487
 Morgan M., Seligman D., Batygin K., 2021, *The Astrophysical Journal Letters*, 917, L8
 Muinonen K., Virtanen J., Bowell E., 2001, *Celestial Mechanics and Dynamical Astronomy*, 81, 93
 Muñoz-Gutiérrez M. A., Peimbert A., Lehner M. J., Wang S.-Y., 2021, *The Astronomical Journal*, 162, 164
 Murray C. D., Dermott S. F., 2000, *Solar System Dynamics*. Cambridge University Press, doi:10.1017/CBO9781139174817, https://www.cambridge.org/core/product/identifier/9781139174817/type/book
 Nakamura T., Kurahashi H., 1998, *The Astronomical Journal*, 115, 848
 Naoz S., Li G., Zanardi M., de Elía G. C., Di Sisto R. P., 2017, *The Astrophysical Journal*, 154, 18
 Nesvorný D., 2018, *Annual Review of Astronomy and Astrophysics*, 56, 137
 Nesvorný D., Youdin A. N., Marschall R., Richardson D. C., 2020, *The Astrophysical Journal*, 895, 63
 Opik E. J., 1951, *Proc. R. Irish Acad.*, 54, 165
 Opik E. J., 1976, *Interplanetary encounters - Close-range gravitational interactions*. Elsevier
 Parisi M. G., Brunini A., 1997, *Planetary and Space Science*, 45, 181
 Pokorný P., Vokrouhlický D., 2013, *Icarus*, 226, 682
 Pokorný P., Sarantos M., Janches D., 2017, *The Astrophysical Journal*, 842, L17
 Rein H., Liu S.-F., 2012, *Astronomy & Astrophysics*, 537, A128
 Rickman H., Winiowski T., Wajer P., Gabryszewski R., Valsecchi G. B., 2014, *Astronomy and Astrophysics*, 569, 1
 Rogozinski Z., Hamilton D. P., 2021, *The Planetary Science Journal*, 2, 78
 Rose S. C., Naoz S., Gautam A. K., Ghez A. M., Do T., Chu D., Becklin E., 2020, *The Astrophysical Journal*, 904, 113
 Schulte P., et al., 2010, *Science*, 327
 Stern S. A., 1995, *The Astronomical Journal*, 110, 856
 Torres S., Cai M. X., Brown A. G. A., Portegies Zwart S., 2019, *Astronomy & Astrophysics*, 629, 13
 Valsecchi G. B., 2005, *Comptes Rendus Physique*, 6, 337
 Vokrouhlický D., Pokorný P., Nesvorný D., 2012, *Icarus*, 219, 150
 Vokrouhlický D., Nesvorný D., Dones L., 2019, *The Astronomical Journal*, 157, 181
 Woo J., Genda H., Brassier R., Mojszsis S., 2019, *Icarus*, 333, 87
 Wyatt M. C., 2008, *Annual Review of Astronomy and Astrophysics*, 46, 339
 Zahnle K., 2001, *Icarus*, 153, 111

APPENDIX A: ÖPIK UNITS

Many studies, following Öpik-like methods, adopted the Jacobi normalized units, in which $G = 1$, $M_s = 1$, the heliocentric distance of the particle at the specified time $r = 1$ and the mean motion $n = 1$. In order to accurately compare with our method and the N-body simulations, we have to bring back the proper units. The Tisserand parameter (Eq. 12) and the relative velocity (Eq. 11) can be rewritten

[h!]

Table B1. Input orbital elements of the particle: a_c , e_c , i_c , Ω_c , ω_c , and f_c , represents the semi-major axis, eccentricity, inclination, longitude of the ascending node, argument of periapsis, and true anomaly of the particle with respect to its orbit about the star.

name	e_c	a_c [au]	i_c [deg]	Ω_c [deg]	ω_c [deg]	f_c [deg]
T-inc	0.1	6	0 – 180	0	0	0
T-ecc	0 – 1	6	2.5	0	0	0

as:

$$T = \frac{GM_s}{a_p} + 2GM_s \sqrt{\frac{a_c(1-e_c^2)}{a_p^3}} \cos i_c \quad (\text{A1})$$

and,

$$U_{\text{opik}}^2 = n^2 a_p^2 + \frac{2GM_s}{a_p} - T, \quad (\text{A2})$$

where n is the mean motion. The relative velocity components are given by,

$$\begin{aligned} U_x &= \pm \sqrt{GM_s \left(\frac{2}{r} - \frac{1}{a_c} - \frac{a_c(1-e_c^2)}{r^2} \right)}, \\ U_y &= \sqrt{GM_s \left(\frac{a_c(1-e_c^2)}{r} \right)} \cos i_c - 1, \\ U_z &= \pm \sqrt{GM_s \left(\frac{a_c(1-e_c^2)}{r} \right)} \sin i_c. \end{aligned} \quad (\text{A3})$$

Finally, using Equations A1, A2 and A3, Eq. 15 can be written as follow,

$$\Gamma_{\text{opik}} = \frac{1}{P} \frac{\sigma_{\text{opik}}^2 U_{\text{opik}}}{\pi a_p^2 \sin i_c U_x}, \quad (\text{A4})$$

where P is the planet's orbital period.

APPENDIX B: COMPARISON WITH THE ÖPIK METHOD

In this section, we compare our method for collision rates with the classic Öpik theory to highlight the flexibility of our formulation. We choose two representative examples, comparing the rates behavior as a function of inclination (**T-inc**) and eccentricity (**T-ecc**) while keeping all other parameters constant. In both cases we choose the semi-major axis, eccentricity and true anomaly of the planet $a_p = 5.2$ au, $e_p = 0.05$, and $f_c = 0^\circ$ respectively, while for the particles we choose the values shown in Table B1. For consistency with Sect. 3.2, we used an inflated radius of collision, $R_p = (M_p/3M_\star)^{1/3} a_p$, where M_\star is the mass of the host star, taken to be one solar mass. We note that the original formulation of Γ_{opik} (Eq. 15) uses Jacobi normalized units. Therefore, in order to proper compare with Γ_{coll} (Eq. 10), we used Γ_{opik} with the proper units (Eq. A4).

In Fig. B1 top panel, we show the collision rates as a function of the particle inclination with respect to the planet at the onset of collision for **T-inc**. The two collision rates exhibit similar functional form as a function of the mutual inclination, i since both are dominated by a similar volume dependency on the mutual inclination $V \sim \sin i$.

In Fig. B1 bottom panel, we show the collision rates as a function of the particle eccentricity at the onset of collision for **T-ecc**. As depicted in Fig. B1 bottom panel, our collision rate Γ_{coll} is qualitatively

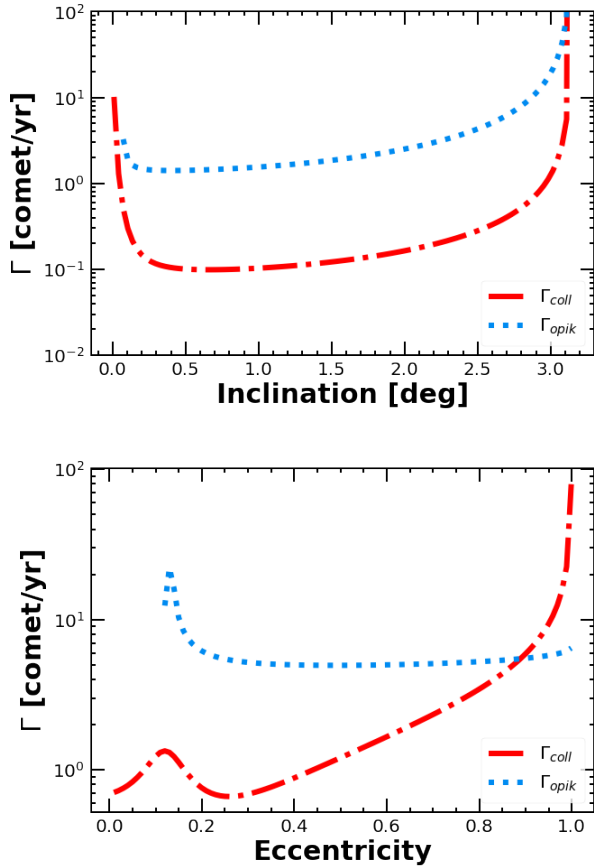


Figure B1. Compression between the Γ_{opik} (dotted blue line) and Γ_{coll} (dash-dot red line). The top panel shows the collision rate as a function of the inclination. While the bottom, the collision rate as a function of the eccentricity.

different from Γ_{opik} . The Öpik method predicts higher collision rates for eccentricities less than ~ 0.85 , and it monotonically decreases from $e = 0$ to $e = 1$. In contrast, Γ_{coll} predicts an increasing distribution with two maximum. The first one for eccentricities within 0 and 0.1. While the second for e_c within 0.4 – 1.

APPENDIX C: N-BODY SIMULATIONS

Following the method describe in Sect.3.2 and using the input parameters shown in Table 1, we preform two set of simulations, **Run-inc** and **Run-ecc**. In **Run-inc** after 10,000 years $\sim 2,123$ particles collided with the planet ($\sim 42.46\%$ of the initial particles). In Fig. C1 we show the distribution of the collided particles, for the semi-major axis (first row), the eccentricity (second row) and the inclination (third row). We find that the particles with inclinations between 0 – 50 and 130 – 160 degrees are the most probable for collision. These particles have eccentricities within 0.4 – 0.6 (see Fig. C1 third column second panel). Additionally, the particles shown a bi-modal distribution in f_c , ω_c and M_c , having their maximums around 100° and 250° (Fig. C2).

In Figures C3 and C4 we show the results of the simulation **Run-ecc**. We find that $\sim 74.84\%$ of the particles remained in the system after 10,000 years. The eccentricity of the collided particles ($\sim 1,258$)

formed a distribution with three peaks with maximums around 0.1, 0.4 and 0.7 (second row Fig. C3). Particles with eccentricity ~ 0.6 did not collide. The longitude of the ascending node Ω_c of the particles has a preferred angle within $-100 - 0$ degrees (second-row Fig. C4). These differed from the distribution of Ω_c in **Run-inc**, where the particles have Gaussian distribution with maximum ~ 0 . Overall, we find that the collided particles in **Run-inc** and **Run-ecc** have a strong dependency in the initial orbital elements, in particular the inclination and eccentricity.

This paper has been typeset from a $\text{\TeX}/\text{\LaTeX}$ file prepared by the author.

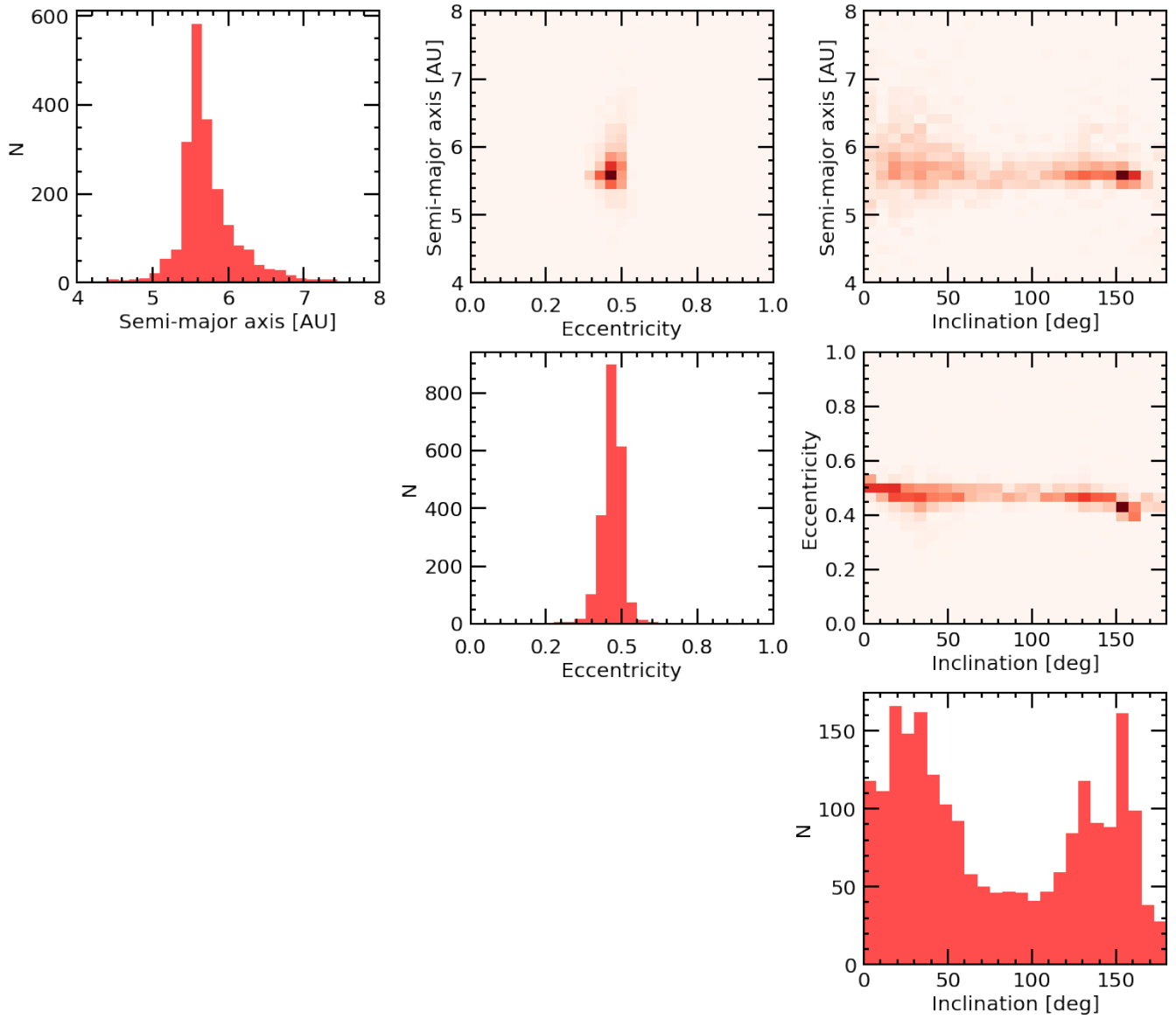


Figure C1. Run-inc. Density map of semi-major axis, eccentricity and inclination of the collided particles.

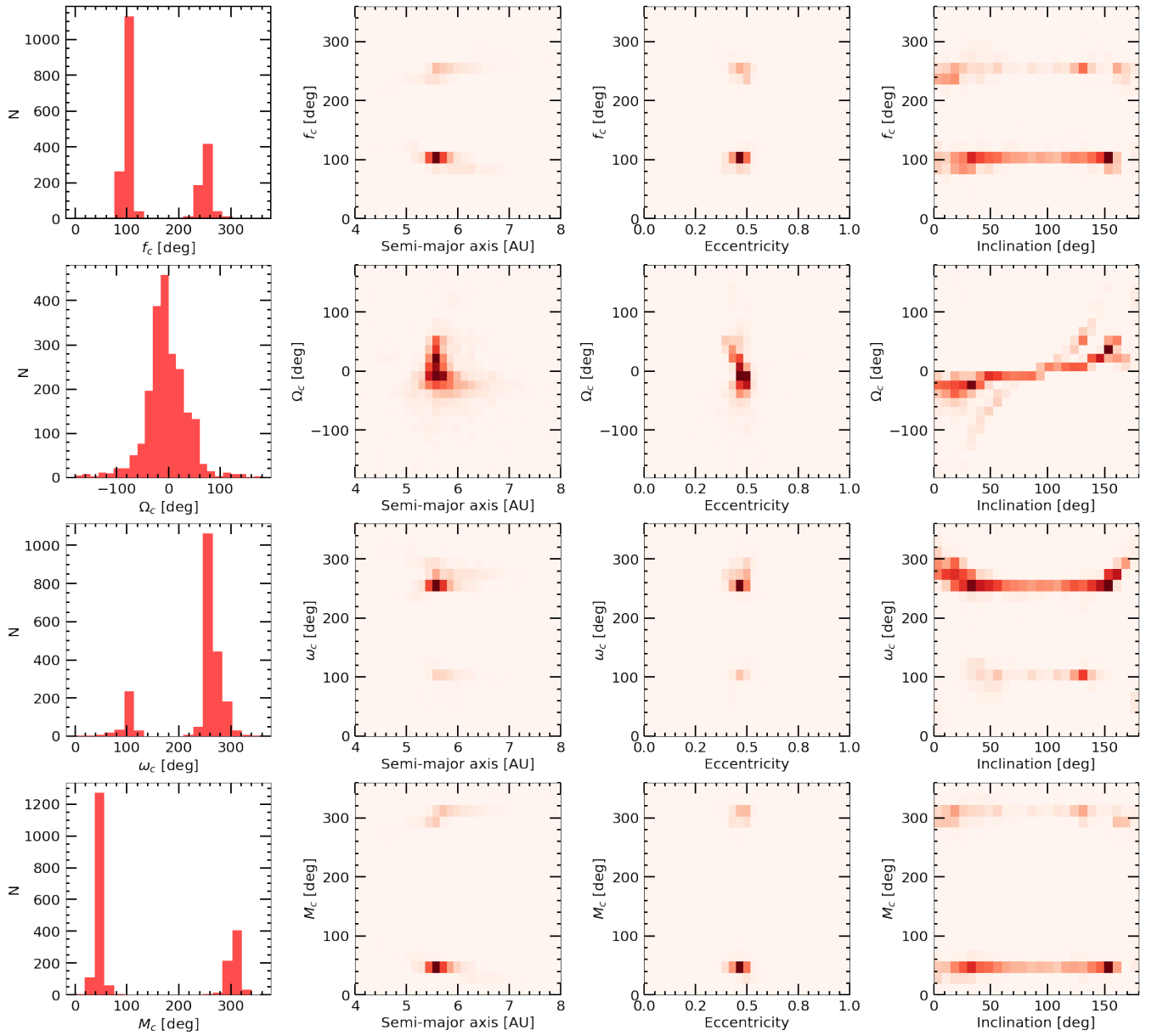


Figure C2. Run-inc. Orbital elements density map of the collided particles. First row, shows the true anomaly f_c as function of the semi-major axis a_c , eccentricity e_c and inclination i_c . Second row, shows the longitude of the ascending node Ω_c as function of a_c , e_c , and i_c . Third row, shows the argument of periastron ω_c as function of a_c , e_c , and i_c . Finally, last row shows the mean anomaly M_c as function of a_c , e_c , and i_c .

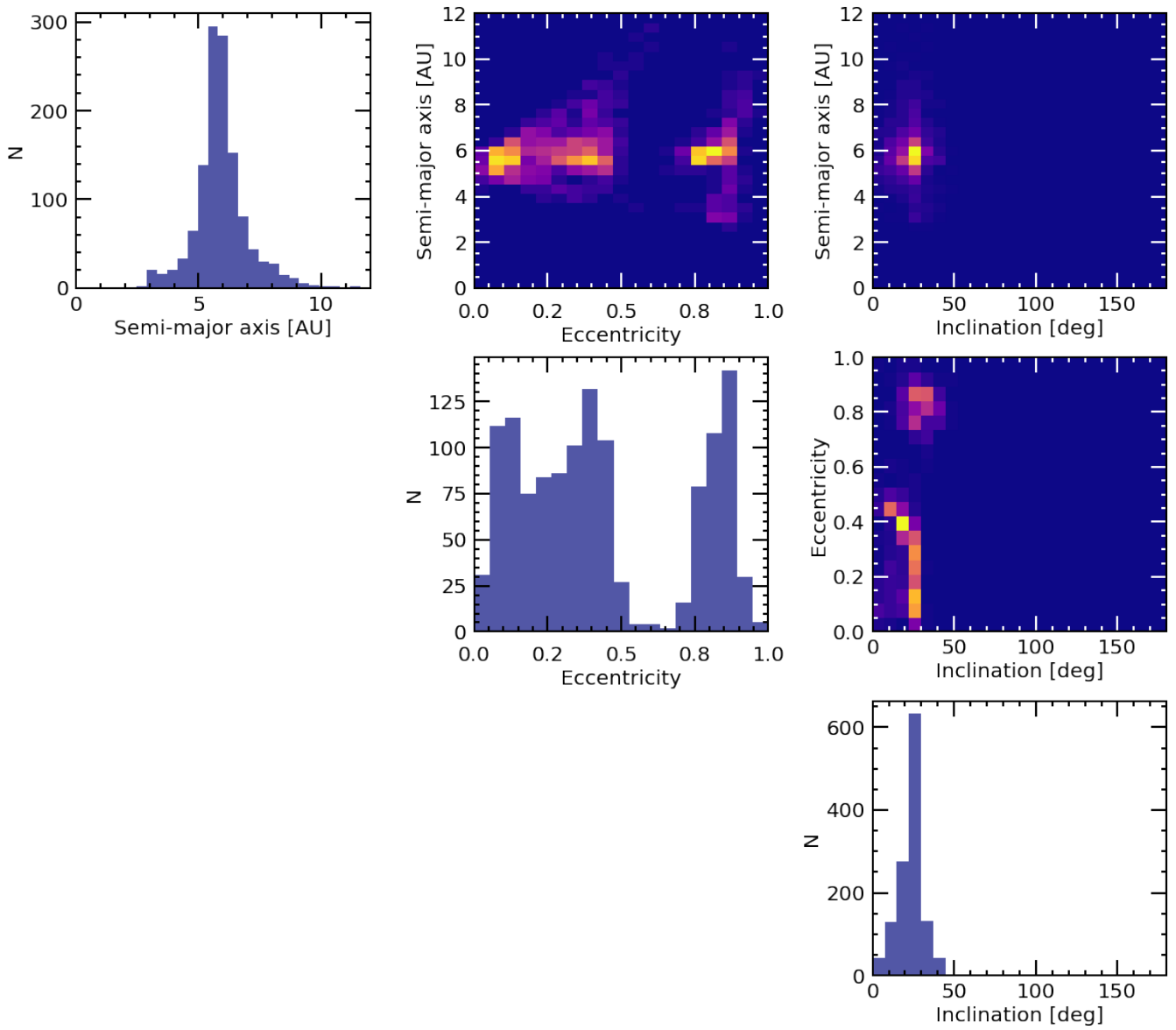


Figure C3. Run-ecc. Density map of Semi-major axis, eccentricity and inclination of the collided particles.

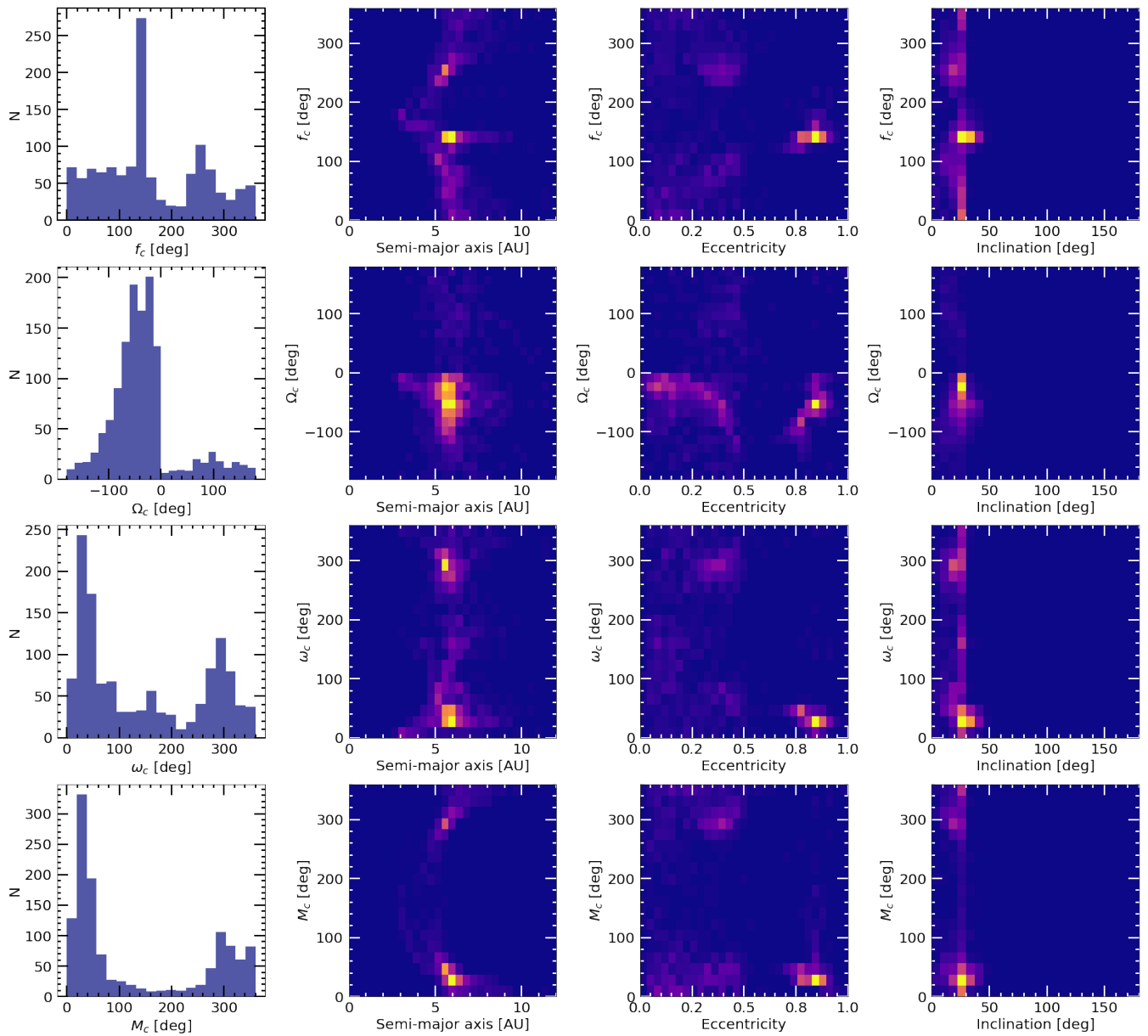


Figure C4. Run-ecc. Orbital elements density map of the collided particles. First row, shows the true anomaly f_c as function of the semi-major axis a_c , eccentricity e_c and inclination i_c . Second row, shows the longitude of the ascending node Ω_c as function of a_c , e_c , and i_c . Third row, shows the argument of periastris ω_c as function of a_c , e_c , and i_c . Finally, last row shows the mean anomaly M_c as function of a_c , e_c , and i_c .